Sphere, Cylinder, and Vesicle Nanoaggregates in Poly(styrene-*b*-isoprene) Diblock Copolymer Solutions

Joona Bang,[†] Sumeet Jain,[†] Zhibo Li,[‡] and Timothy P. Lodge*[,†,‡]

Department of Chemical Engineering & Materials Science and Department of Chemistry, University of Minnesota, Minneapolis, Minnesota 55455-0431

Jan Skov Pedersen

Department of Chemistry, University of Aarhus, DK-8000 Aarhus C, Denmark

Ellina Kesselman and Yeshayahu Talmon

Department of Chemical Engineering, Technion-Israel Institute of Technology, Haifa 32000, Israel

Received September 16, 2005; Revised Manuscript Received November 1, 2005

ABSTRACT: An asymmetric poly(styrene-*b*-isoprene) diblock copolymer with block molecular weights of 13 000 and 71 000 g/mol, respectively, was dissolved at 1 vol % in a series of solvents with varying selectivity for styrene: dibuthyl phthalate (DBP), diethyl phthalate (DEP), and dimethyl phthalate (DMP). The degree of solvent selectivity was adjusted by mixing DBP/DEP and DEP/DMP in various proportions. With increasing solvent selectivity, the predominant micellar shape changes from spheres to cylinders to vesicles, reflecting the changing interfacial curvature. The detailed micellar morphologies were characterized by small-angle X-ray scattering (SAXS) and cryogenic transmission electron microscopy (cryo-TEM). Recently developed form factors were used to characterize the micellar structures in detail, and a vesicle form factor was derived for this system. From the core dimensions, the packing properties, such as the interfacial area per chain and the core chain stretching, were determined. The cryo-TEM results demonstrate the suitability of the technique for these glass-forming solvents and gave micellar core dimensions in quantitative agreement with those from SAXS. The universality of the shape sequence sphere/cylinder/vesicle, well-established for aqueous solutions of surfactants and block copolymers, is thus confirmed for organic systems.

Introduction

As macromolecular surfactants, block copolymers have been shown to self-assemble into various microstructures. They offer certain potential advantages over small-molecule surfactant systems, as the micellar size and the architecture, as well as the chemical nature, can be readily tuned by synthesis, and the resulting nanostructures can be remarkably robust. Many recent studies have focused on aqueous systems, in which the strongly amphiphilic characteristics of the polymers lead to various micellar shapes (spheres, cylinders, vesicles, compound micelles, etc.).[1−3]

Micellar morphology in nonionic copolymers is generally determined by a force balance among three contributions to the free energy:[4] core chain stretching, corona chain repulsion, and the core/corona interfacial tension. Although intrinsic properties such as the block−block interaction parameter, χ, play an important role in balancing these contributions, it is not a readily tunable factor for a given system. However, extrinsic properties such as overall molecular weight, block composition, and solvent quality can be adjustable. Two extensive, systematic studies have shown that this balance of forces can be controlled by changing either the block composition or the solution conditions, resulting in morphological transitions between spheres, cylinders, and vesicles. Won et al. studied nonionic poly(butadiene-*b*-oxyethylene) (PB−PEO) diblock copolymers in water.[2] As the length of the hydrophilic PEO block increased, the morphological sequence from vesicles to cylinders to spheres was observed. In this case, the key contribution is the corona chain repulsion, as the corona PEO block was varied to control the micellar morphology. This transition can be also anticipated from molecular packing considerations,[5] in that increasing the hydrophilic block increases the natural interfacial curvature. The Eisenberg group investigated poly(styrene-*b*-acrylic acid) (PS−PAA) ionic diblock copolymers in mixtures of water/dioxane or water/dimethylformamide (DMF).[6−10] The solvent quality was adjusted by adding water during dialysis. A transition from spheres to cylinders to vesicles was achieved by increasing the fraction of water in the mixture, thereby increasing the interfacial tension. The presence of additives such as ions, surfactants, and homopolymers could also be used to control the size and the shape of the micelle.

In contrast to aqueous solutions, observations of nonspherical micelles in organic solutions are rare, albeit with a few exceptions.[11−14] Canham et al. dispersed a poly(styrene-*b*-butadiene-*b*-styrene) (SBS) triblock copolymer in ethyl acetate.[11] The solutions showed a distinct cloud point upon heating, and they found that the onset of cloudiness was due to the formation of long cylinders from spheres. Recently, LaRue et al. found that cylindrical micelles can form from poly(styrene-*b*-isoprene) (SI) diblock copolymers in heptane.[13,14] It was shown that the morphology changed from spheres to cylinders by reducing the length of the isoprene corona block, analogous to the work of Won et al. in aqueous systems. The same group has also inferred the presence of vesicles in the same system.[15] In a closely related system, Pedersen et al. studied a highly asymmetric SI diblock copolymer in dibutyl phthalate (DBP), a solvent selective for

[†] Department of Chemical Engineering & Materials Science.
[‡] Department of Chemistry.
* Author for correspondence: e-mail lodge@chem.umn.edu.

10.1021/ma052023+ CCC: $33.50
Published on Web 01/04/2006

the shorter styrene block.[12] From small-angle neutron (SANS) and X-ray (SAXS) scattering, it was concluded that the micellar cores were significantly swollen by solvent, and the micellar shape was a prolate ellipsoid. As an effect of the polymer architecture on the micellar morphology, Putaux et al. recently demonstrated that the cyclic SI copolymer can form vesicles whereas the analogous linear copolymer adopts spherical micelles.[16] In this paper we report the systematic morphological change from spheres to cylinders to vesicles for a styrene−isoprene diblock copolymer, by varying the solvent selectivity and thus the interfacial tension between the core and the solvated corona. A preliminary account of the formation of vesicles, as characterized by cryogenic transmission electron microscopy (cryo-TEM), has been given.[17,18]

In characterizing micellar morphology, cryo-TEM and small-angle scattering (SAXS and SANS) techniques have been proven to be very suitable tools.[1,19,20] The cryo-TEM technique is particularly powerful, as it provides direct images, and it is well established in aqueous systems.[2,19,21,22] However, cryo-TEM has been applied to organic systems only rarely.[17,18,23,24] This is due in part to the difficulty in solvent vitrification, as many organic solvents dissolve in liquid ethane, the cryogen of choice. Alternatively, a freeze-drying TEM technique has been used.[25] Fortunately, the solvents used in the present work, a series of dialkyl phthalates, turn out to be readily vitrified with liquid nitrogen as they are glass-formers, and thus cryo-TEM could be used in these solvents. SAXS and SANS are more suitable than cryo-TEM for detailed, quantitative information on the equilibrium solution structure, provided an appropriate fitting model is available. In this work, the samples shown by cryo-TEM to have spherical, cylindrical, and vesicular aggregates were measured by SAXS and fitted by corresponding model form factors. The results from both techniques were compared to confirm the nanoaggregate morphologies.

Experimental Section

Materials. An asymmetric poly(styrene-*b*-isoprene) diblock copolymer with block molecular weights of 1.3×10^4 and 7.1×10^4 g/mol, respectively, was polymerized by living anionic polymerization using standard procedures and designated SI(13-71).[26] The polymer was characterized by size exclusion chromatography (SEC), using both refractive index (Wyatt Optilab) and multiangle light scattering detectors (Wyatt Dawn), and by nuclear magnetic resonance spectroscopy (^{1}H NMR). SEC determined the number-average block molecular weights, M_{PS} and M_{PI}, and the polydispersity, $M_w/M_n = 1.02$. ^{1}H NMR was used to determine the block composition and to estimate the mole percent of 4,1-addition of the PI block (94 ± 1%). The solvents di-*n*-butyl phthalate (DBP), diethyl phthalate (DEP), and dimethyl phthalate (DMP) were purchased from Aldrich and purified by vacuum distillation. Polymer solutions were prepared gravimetrically, with the aid of methylene chloride as a cosolvent. The cosolvent was stripped off under a stream of nitrogen at room temperature until a constant weight was achieved. The polymer volume fraction, ϕ, was maintained at 0.01 in the pure solvents and in various mixtures of DBP/DEP and DEP/DMP. The concentrations were calculated assuming additivity of volumes and densities of 1.043, 1.118, 1.160, 1.047, and 0.913 g/cm^3 for DBP, DEP, DMP, PS, and PI, respectively.

Small-Angle X-ray Scattering (SAXS). SAXS measurements were performed using beamline 5ID-D, in the DuPont-Northwestern-Dow (DND-CAT) Synchrotron Research Center at the Advanced Photon Source, Argonne National Laboratory. An energy of 15 keV, corresponding to a wavelength $\lambda = 0.83$ Å, was selected from an undulator beam using a double-crystal monochromator and then collimated using two sets of adjustable slits. The data were collected using a CCD detector (MAR) having a maximum resolution of 2048×2048 pixels (78.75×78.75 μm^2 pixel size) with a 16-bit intensity scale and a circular active area of 133 mm diameter. A sample-to-detector distance of 3.1 m was used to access the necessary q range. Silver behenate (Dupont) was used as a calibrant for q ($d_{001} = 58.380$ Å).

The $\phi = 0.01$ solutions were sealed within 2.0 mm quartz capillaries with a high-temperature silicone-based sealant. These samples were put in an evacuated sample chamber. All measurements were taken at ambient temperature with exposure times of 60−180 s. The 2-D SAXS images were azimuthally averaged to produce one-dimensional profiles of intensity, I, vs wavevector, q, using the two-dimensional data reduction program FIT2D. The solvent backgrounds from pure solvents or solvent mixtures were also collected, and the scattering data at higher q values were normalized and then subtracted from the corresponding solution data. No attempt was made to convert the data to an absolute scale.

Cryogenic Transmission Electron Microscopy (Cryo-TEM). Various solutions were examined by cryo-TEM. A small droplet of the solution was placed on a perforated carbon film supported on a TEM copper grid, held by tweezers. It was then blotted by a piece of filter paper, resulting in the formation of thin films of 100−300 nm thickness within the micropores in the carbon-coated lacelike polymer layer supported on the grid. After blotting, the sample was allowed to relax any possible deformation that may result from flow during the blotting process. The specimen was then plunged into a reservoir of liquid nitrogen. The vitrified specimen was transferred under liquid nitrogen and mounted on a cryogenic sample holder. All samples were observed under low-dose conditions. Some images were acquired using a JEOL 1210 TEM operating at 120 kV equipped with a Gatan 626 cryo-holder. Adequate phase contrast was obtained at a nominal underfocus of 2−4 μm. Images were recorded on a Gatan Multiscan 724 digital camera and processed with DigitalMicrograph version 3.3.1 software. The ramp-shaped optical density gradients in the background were digitally corrected. Other vitrified samples were examined in an FEI T12 G^2 Cryo-TEM, equipped with an Oxford CT-3500 cryo-holder system and a Gatan US1000 high-resolution cooled CCD camera.

Models. To fit the SAXS data, the scattering form factors of block copolymer micelles with sphere, cylinder, and vesicle shapes comprising a homogeneous core and corona chains attached to the core surface were employed.[27,28] In general, these models contain four different terms: the self-correlation of the core, the self-correlation of the corona chains, the cross term between the core and corona chains, and the cross term between different corona chains. The resulting form factor $P_{mic}(q)$ can be expressed as a general form:

$$P_{mic}(q) = Q^2\beta_{core}{}^2A_{core}{}^2(q) + Q(Q-1)\beta_{corona}{}^2A_{corona}{}^2(q) + 2Q^2\beta_{core}\beta_{corona}A_{core}(q)A_{corona}(q) + Q\beta_{corona}{}^2P_{chain}(q) \quad (1)$$

where q is the scattering vector, Q is the aggregation number, and β_{core} and β_{corona} are the total excess scattering lengths of a core and corona block, respectively. These are defined as $\beta_{core} = v_{core-block}(\rho_{core-block} - \rho_{sol})$ and $\beta_{corona} = v_{corona-block}(\rho_{corona-block} - \rho_{sol})$, where v_x is the volume of the core or corona block and $\rho_{core-block}$, $\rho_{corona-block}$, and ρ_{sol} are the scattering length density of the core block, the corona block, and the solvent, respectively. Also, $A_{core}(q)$ and $A_{corona}(q)$ represent the form factor amplitudes of core and corona according to the micellar shape, respectively, and $P_{chain}(q)$ is the form factor of the corona chains.

Spherical Micelles. For a homogeneous spherical core with radius R_c and a smoothly decaying scattering length density at the core surface, the core term is

$$A_{core}{}^2(q) = \Phi^2(qR_c)\exp(-q^2\sigma^2) \quad (2)$$

where $\Phi(x) = 3[\sin x - x\cos x]/x^3$ is the form factor amplitude of a solid sphere, with $x = qR_c$. The exponential term reflects a

smoothly decaying density at the core surface, and σ is related to the width of the interface.

The corona chain self-correlation term for Gaussian chains with radius of gyration R_g is given by the Debye function:

$$P_{chain}(q) = \frac{2[\exp(-x) - 1 + x]}{x^2} \quad (3)$$

where $x = q^2R_g^2$. In this work, the corona term was modeled with noninteracting Gaussian chains in the corona:

$$A_{corona}(q) = \psi(q^2R_g^2)\left(\frac{\sin[q(R_c + dR_g)]}{q(R_c + dR_g)}\right)\exp(-q^2\sigma^2/2) \quad (4)$$

where $\psi(x) = [1 - \exp(-x)]/x^2$, with $x = q^2R_g^2$. In this equation d is close to unity ($d \approx 1$), as this mimics nonpenetration of the corona chains into the core region. In other words, the center of mass of the corona chains is on a surface at $R_c + dR_g$, and not at R_c. This corresponds to a "mushroom-like" structure of the coronal chains. While this model has a simple form, the corresponding radial profile is not in all cases well-defined, as there can be overlap between core and corona. Hence, this model can be useful only when the corona contribution is narrow relative to the core, i.e., $R_g \ll R_c$. For a corona contrast system, a more elaborate description of the corona chains is needed, such as a sum of cubic spline function, as described previously.[29]

Cylindrical Micelles. For a micelle with a cylindrical core of radius R_c and length L, the form factor amplitudes of the core and the corona need to be averaged over all orientations relative to the scattering vector q. Equation 1 is then modified as follows:[28]

$$P_{mic}(q) = Q^2\beta_{core}^2\langle A_{core}^2(q,R_c,L,\theta)\rangle + Q(Q-1)\beta_{corona}^2\langle A_{corona}^2(q,R_c,L,\theta)\rangle + 2Q^2\beta_{core}\beta_{corona}\langle A_{core}(q,R_c,L,\theta)A_{corona}(q,R_c,L,\theta)\rangle + Q\beta_{corona}^2P_{chain}(q) \quad (5)$$

where $\langle\ \rangle$ represents the orientational average such that $\langle f\rangle = \int_0^{\pi/2} f(\theta)\sin\theta\, d\theta$, and θ is the angle of the long axis of cylinder oriented with respect to q. The form factor amplitude has the well-known form

$$A_{core}(q,R_c,L,\theta) = \frac{2J_1(qR_c\sin\theta)}{qR_c\sin\theta}\frac{\sin\left(\frac{qL}{2}\cos\theta\right)}{\frac{qL}{2}\cos\theta} \quad (6)$$

where $J_1(x)$ is the first-order Bessel function of the first kind.

As with spheres, the corona term was also modeled with the noninteracting Gaussian chains.[28] In the present work, it was assumed that the Gaussian chains were at dR_g away from the surface of the cylinder core, i.e., radius of $R + dR_g$ on the cylinder wall and $L + 2dR_g$ on the cylinder ends. The corona form factor amplitude, $A_{corona}(q)$, is then decomposed into two terms that describe the scattering from the circular end-disks, $A_{corona}^{end}(q)$, and the cylinder wall, $A_{corona}^{cross}(q)$. They are defined as

$$A_{corona}^{cross}(q,R_c,L,\theta) = \frac{2J_1(qR_c\sin\theta)}{qR_c\sin\theta}\cos\left(\frac{qL}{2}\cos\theta\right) \quad (7)$$

$$A_{corona}^{end}(q,R_c,L,\theta) = J_0(qR_c\sin\theta)\frac{\sin\left(\frac{qL}{2}\cos\theta\right)}{\frac{qL}{2}\cos\theta} \quad (8)$$

where $J_0(x)$ and $J_1(x)$ are the zeroth- and first-order Bessel functions of the first kind, respectively. With the appropriate weighting factors, $A_{corona}(q)$ is then

$$A_{corona}(q,R_c,L,\theta) = \psi(qR_g)\left[\frac{L}{R_c+L}A_{corona}^{cross}(q, R + dR_g, L + 2dR_g, \theta) + \frac{R_c}{R_c+L}A_{corona}^{end}(q, R + dR_g, L + 2dR_g, \theta)\right] \quad (9)$$

where again $\psi(x) = [1 - \exp(-x)]/x^2$.

Bilayer Vesicles. The form factor for the bilayer vesicle was derived from the hollow sphere model with corona chains attached both inside and outside the core. In this case, the core scattering amplitude represents the Fourier transform of the radial scattering length density distribution of the core with outer radius R_{out} and inner radius R_{in}, and the core contribution in eq 1, $Q\beta_{core}A_{core}(q)$ in the first and third terms, is then replaced by

$$A_{core,vesicle}(q) = \beta_{core}[V_{out}\Phi(qR_{out}) - V_{in}\Phi(qR_{in})]\exp(-q^2\sigma^2/2) \quad (10)$$

where $V_{out} = 4\pi/3R_{out}^3$ and $V_{in} = 4\pi/3R_{in}^3$, and $\Phi(x) = 3[\sin x - x\cos x]/x^3$ is the hard-sphere form factor. In terms of the radius of the center of the vesicle R and half the width of the vesicle core L_c one has $R_{out} = R + L_c$ and $R_{in} = R - L_c$.

For noninteracting Gaussian chains it is straightforward to derive the amplitude of the corona form factor:

$$A_{corona}(q,R,L_c) = \psi(qR_g)\frac{1}{2}\left[\frac{\sin[q(R + L_c + dR_g)]}{q(R + L_c + dR_g)} + \frac{\sin[q(R - L_c - dR_g)]}{q(R - L_c - dR_g)}\right] \quad (11)$$

In the present work we have chosen to use another radial profile based on partial cubic b spline.[29] The reason for this is that a significantly more pronounced chain−chain interaction is expected in the corona of the vesicle compared to the more curved surfaces of spherical and cylindrical micelles. The enhanced chain−chain interaction is expected to give a brushlike profile, as described by the splines and as opposed to the mushroom-like profile of the noninteracting Gaussian chain model (see also discussion below).

As mentioned, the radial profiles of the corona were described by a sum of partial cubic b spline functions.[29−31] $A_{corona}(q)$ is then given as the normalized Fourier transform of the radial density distribution function of the corona chains, $\rho_{corona}(r)$, as follows:

$$A_{corona}(q) = \frac{4\pi\int\rho_{corona}(r)\frac{\sin(qr)}{qr}r^2\,dr}{4\pi\int\rho_{corona}(r)r^2\,dr}\exp(-q^2\sigma^2/2) \quad (12)$$

In this work we have chosen to represent $\rho_{corona}(r)$ as a linear combination of two cubic b splines, as has been successfully applied previously,[29−32] and the number of fitting parameters increases by only one compared to the noninteracting Gaussian chain model. The explicit form of $\rho_{corona}(r)$ and the corresponding transformations are described in the Appendix.

Polydispersity. To account for polydispersity, a Gaussian or an exponential distribution was used. The core size of spheres R_c and the overall size of vesicles R were assumed to follow a Gaussian distribution in the fit.

$$D(R_c) = \frac{1}{\sqrt{2\pi}\sigma_R}\exp\left[\frac{-(R_c - \langle R_c\rangle)}{2\sigma_R^2}\right] \quad \text{for } R_c > 0 \quad (13)$$

where $\langle R_c\rangle$ is the average radius and σ_R is the standard deviation of the distribution.

For cylinders the polydispersity of the length L rather than the core radius R_c was considered, as it is known that L often has a much broader distribution. Cates et al. predicted an exponential distribution for the number of chains of length L, from the consideration of the breakage−recombination process in living polymers.[33] In this case the distribution of L, in terms of volume,

can be expressed as

$$D(L) = \frac{L}{\langle L \rangle^2} \exp\left[-\frac{L}{\langle L \rangle}\right] \quad \text{for } L > 0 \tag{14}$$

where $\langle L \rangle$ is the average length of cylinders. The resulting distribution is essentially analogous to a Schulz distribution with a variance $\sigma L/\langle L \rangle = 1$. In this paper we will refer to this distribution as an "exponential" distribution to designate the origin of this distribution. Note that this "exponential" distribution is asymmetric and is skewed toward larger particle sizes. Also, we considered a Gaussian distribution for L and compared the results.

The coherent scattering intensity for the polydisperse model is then given by

$$I(q) = \int P_{\text{mic}}(q) D(R_c)\, \mathrm{d}R_c, \quad \text{for spheres}$$

$$I(q) = \int P_{\text{mic}}(q) D(R)\, \mathrm{d}R, \quad \text{for vesicles}$$

where a constant thickness L_c is assumed for vesicles and

$$I(q) = \int P_{\text{mic}}(q) D(L)\, \mathrm{d}L, \quad \text{for cylinders} \tag{15}$$

Results and Discussion

General Comments. The dialkyl phthalates DBP, DEP, and DMP are all styrene-selective but differ in the degree of selectivity. In other words, they are all good solvents for polystyrene but have different theta temperatures for polyisoprene. A decrease in the alkyl chain length increases the preference for styrene, and thus DBP is slightly selective at room temperature, DEP is more selective, and DMP is strongly selective. As an ongoing effort, we have explored in detail the effect of the solvent selectivity of dialkyl phthalates on the phase behavior of SI diblock copolymer solutions.[26,34−36] For a series of polymers of varying composition, order−order (OOT) and order−disorder transitions (ODT) were located, and the phase diagrams were constructed as a function of temperature (0−250 °C) and concentration ($0 \le \phi \le 1$) in pure DBP, DEP, and DMP. Overall, the phase behaviors in those solvents were similar, in that they showed the same trends in terms of lyotropic and thermotropic transitions, with the main differences being shifts of the phase boundaries with solvent. As the solvent selectivity increases, the solvent will more preferentially segregate into the favored styrene domain, and the interfacial tension between isoprene and styrene + solvent increases. For the same reason, the critical micelle temperature (cmt) in dilute solution also increases as the selectivity increases. For example, several SI diblocks showed cmt's below 0 °C (DBP), near 75 °C (DEP), and near 150 °C (DMP).[26]

The key aspect of this study is the change of interfacial curvature with respect to solvent selectivity in dilute solution. As the solvent becomes more selective, the interfacial tension should increase, leading to a decrease in the area per chain, and increases in the core chain stretching and corona overlap. When the chain−chain repulsion within the corona is small enough, the interfacial curvature can be reduced, and hence micellar shape changes from spheres to cylinders to vesicles are expected. However, we have previously not observed anything other than spherical micelles in various SI diblock copolymers, over the composition range $0.23 < f_{PS} < 0.70$.[26,34−36] The effect of increasing the solvent selectivity for these polymers was an increase in the cmt, but without a change in the micellar shape. This implies that the PS corona chain repulsion at this f_{PS} range overcomes the interfacial tension and prevents any change in the interfacial curvature. When SI copolymers become more asymmetric (reducing f_{PS}) so that the PS corona chain repulsion is less significant, one might anticipate the curvature change induced by the increase in the interfacial tension. As noted previously, we have reported prolate ellipsoidal micelles in highly asymmetric SI copolymers, i.e., $f_{PS} = 0.16-0.17$, in DBP.[12] This suggests that the interfacial tension is just beginning to overcome the PS corona chain repulsion at this f_{PS} range.

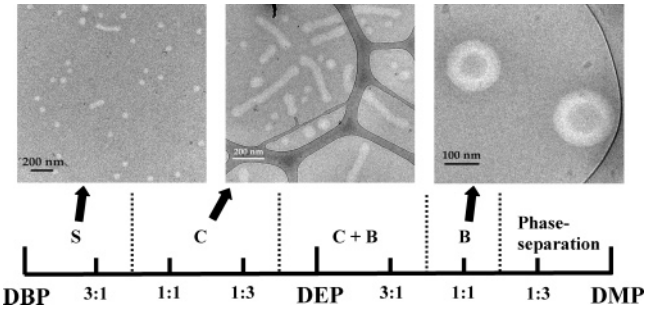

Figure 1. Morphology diagram of SI(13-71) in various dialkyl phthalates with $\phi = 0.01$ at ambient temperature, as a function of the solvent selectivity. The micellar structures of spheres (S), cylinders (C), and bilayer vesicles (B) are clearly identified by cryo-TEM images. The boundaries between morphologies, based on SAXS fits, are only approximate; coexistence (S/C and C/B) is the rule rather than the exception.

TEM Images. Here we studied a slightly more asymmetric SI diblock copolymer, SI(13−71) with $f_{PS} = 0.15$, in a series of dialkyl phthalates and their mixtures. DBP, DEP, and DMP are completely miscible, and the solvent selectivity can be adjusted continuously by mixing these solvents. As the solvent selectivity has been shown to affect the position of phase boundaries (OOT, ODT, and cmt), we can manipulate transition temperatures for experimental convenience.[37] For example, the fcc to bcc OOT for SI(15-15) in DEP with $\phi = 0.20$ occurs at 90 °C, but the use of a 1:1 mixture of DEP and DBP moved it to 45 °C. In this work mixtures of DBP/DEP and DEP/DMP were prepared in different ratios, and the solvent selectivity was modified incrementally at room temperature.

Figure 1 summarizes the morphological diagram for SI(13-71) in various dialkyl phthalates and their mixtures with $\phi = 0.01$ as a function of the solvent selectivity, as well as representative cryo-TEM images. The micellar shapes were determined conclusively by a combination of SAXS data and cryo-TEM images. In pure DBP and a 3:1 mixture of DBP/DEP spherical micelles predominate. By increasing the portion of DEP, a shape transition from spheres to cylinders was induced. The lengths of the cylinders displayed in the accompanying cryo-TEM image are relatively short (<500 nm) comparing to the long wormlike micelles (>1 μm) reported in aqueous systems[2,21] and LaRue's work.[13,14] We have not observed such long cylinders, probably due to a relatively small penalty for forming a spherical end-cap. This could result from the relatively weakly segregated core−corona interface and also the relatively high molecular weight.[22,38] The slightly expanded spherical end-caps are visible in the image, as are some spherical micelles. Upon increasing the solvent selectivity further, the coexistence of cylinders/vesicles (in pure DEP and DEP/DMP-[3:1] mixture) and vesicles (DEP/DMP[1:1] mixture) are observed, and finally, in DEP/DMP[1:3] and pure DMP the solutions phase-separate.

The images in Figure 1 reveal an interesting feature, as noted previously for vesicles.[18] The PI cores appear lighter than the solvent background, i.e., a "reverse" contrast, which has not been observed in aqueous systems. This feature is attributable to the higher electron density of the dialkyl phthalates compared to the PS and PI blocks (0.565 and 0.509 mol e^-/cm^3,

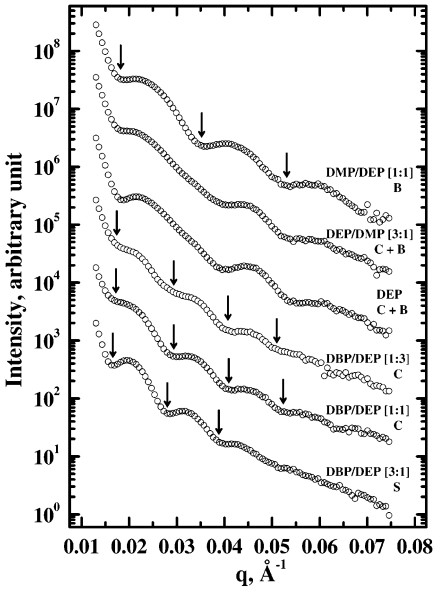

Figure 2. SAXS data as a function of solvent selectivity for SI(13-71) in various dialkyl phthalates with $\phi = 0.01$ at ambient temperature. For clarity, the data have been multiplied by 10, 10^2, 10^3, 10^4, and 10^5, respectively. The arrows indicate the positions of the form factor minima.

respectively). Note that the electron density of dialkyl phthalates is also higher than water (0.555 mol e$^-$/cm^3). Also, the electron density increases from DBP (0.562 mol e$^-$/cm^3) to DEP (0.594 mol e$^-$/cm^3) to DMP (0.625 mol e$^-$/cm^3), and hence "reverse" contrast is facilitated in DEP/DMP[1:1] solutions. As also noted previously,[18] upon prolonged exposure the contrast is reversed, i.e., the micelles become darker than the surrounding medium, due to radiolytic damage. For vesicles we demonstrated that the size and shape of the aggregates are preserved during this process.[18] The same is true for spheres and cylinders (data not shown).

SAXS Results and Modeling. Figure 2 displays the SAXS data for $\phi = 0.01$ solutions of SI(13-71) in various dialkyl phthalates, measured at ambient temperature. All the scattering data feature distinct form factor minima. Since the volume fraction of the PI core block is much higher than PS corona block, and the core contrast for SAXS is also greater than the corona contrast, one can expect that the scattering intensities are mainly due to the core scattering. In this case, the distinct minima of the form factors reflect the core dimension; the core radius (R_c) for spheres and cylinders and the half layer thickness (L_c) for vesicles. The core dimensions can be estimated using the characteristic equations for the form factor minima without detailed modeling. They are

$$\tan(qR_c) - qR_c = 0, \quad \text{for spheres}$$
$$J_1(qR_c) = 0, \quad \text{for cylinders}$$
$$\sin(qL_c) = 0, \quad \text{for vesicles} \qquad (16)$$

With these equations and the q values corresponding to the form factor minima (indicated as arrows in Figure 2), R_c and L_c were estimated to be 28 nm for spheres, 25 nm for cylinders, and 17 nm for vesicles (see Table 1). These values were then used as initial input in the detailed modeling.

There are two scattering curves (SI(13-71) in DEP and in DEP/DMP[3:1]) which cannot be assigned to a single morphology. They show a broadened first maximum, followed by a distinct second maximum. Since the minima do not correspond

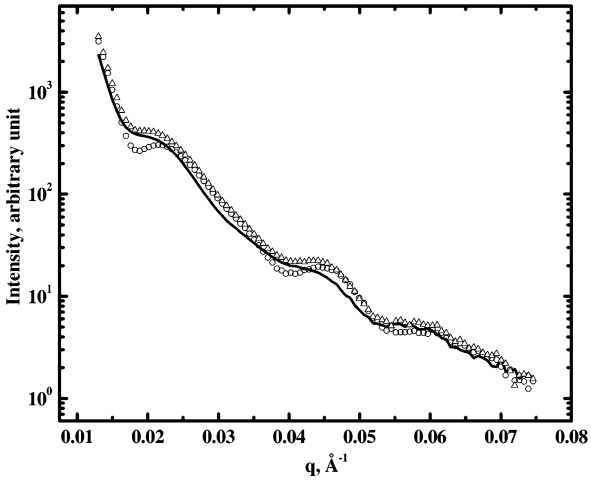

Figure 3. Superimposed SAXS data for SI(13-71) in DEP and DEP/DMP[1:3] $\phi = 0.01$ at ambient temperature (circles). The solid line is a result of averaging SAXS data for SI(13-71) in DBP/DEP[1:1] and DEP/DMP[1:1], which are the representative examples of form factors for cylinders and vesicles, respectively.

to any of the three micellar morphologies, and they are observed between cylinders and vesicles, it is very likely that the scattering patterns are a result of a mixture of cylinders and vesicles. The form factor of the mixture can be expressed as

$$P(q)_{mix} = \phi_{cyl}P(q)_{cyl} + (1 - \phi_{cyl})P(q)_{vesicle} \qquad (17)$$

where ϕ_{cyl} is the number fraction of cylinders. On the basis of this equation, the scattering patterns of SI(13-71) in DEP and DEP/DMP[3:1] solutions were approximated by a sum of the SAXS patterns of SI(13-71) in DBP/DEP[1:1] (cylinders) and DEP/DMP[1:1] (vesicles) solutions. As seen in Figure 3, a sum of these data, shown as the solid line, gives a reasonable description of the form factors of the mixture when $\phi_{cyl} \approx 0.5$, implying that cylinders and vesicles coexist in comparable proportions. (The cryo-TEM images confirm the prevalence of coexistence of two morphologies in almost all the solutions examined, but it is not possible to obtain reliable estimates of the relative populations in this manner due to the small sample size.)

At finite concentrations the interparticle interference effects can be described by a structure factor. However, since the SAXS data were obtained at low concentration ($\phi = 0.01$) to minimize the effect of intermicellar correlations, and peaks from the structure factor were not observed in the q range of the data, the structure factor was not considered in the modeling. Furthermore, the SAXS patterns are dominated by the core scattering. For example, $\beta_{corona}^2/\beta_{core}^2$ is 3×10^{-4} for spheres (DBP/DEP[3:1] solution), 1×10^{-3} for cylinders (DBP/DEP-[1:1] solution), and 5×10^{-3} for vesicles (DEP/DMP[1:1] solution). The difference above is due to the increase in the electron density from DBP to DEP to DMP. The sphere and cylinder models were, therefore, simplified by considering the corona as Gaussian chains. A sum of two spline functions was used for the corona profile of the vesicles, as the corona contribution is larger.

Figure 4a shows the result of the spherical micelle fit for the DBP/DEP[3:1] solution. The fitting parameters are the core radius, R_c, the radius of gyration of the corona chain R_g, and the width of the core size distribution, σ_R. The displacement of the corona chain d was fixed at unity. The other parameters, such as the number density of particles and the aggregation numbers, were considered as arbitrary prefactors, as the SAXS

Table 1. Characteristics of SI(13-71) Assemblies in Dialkyl Phthalates

solvent	morphology	R_c [a] (nm)	R_c [b] (nm)	R_c [c] (nm)	a_0 (nm^2/chain)	s
DBP/DEP [3:1]	sphere	28	29	28	13	1.32
DBP/DEP [1:1]	cylinder	25	25	27	11	1.14
DEP/DMP [1:1]	vesicle	17	18	20	8	0.82

[a] From $P(q)$ minima estimation. [b] From SAXS fits. [c] From cryo-TEM images.

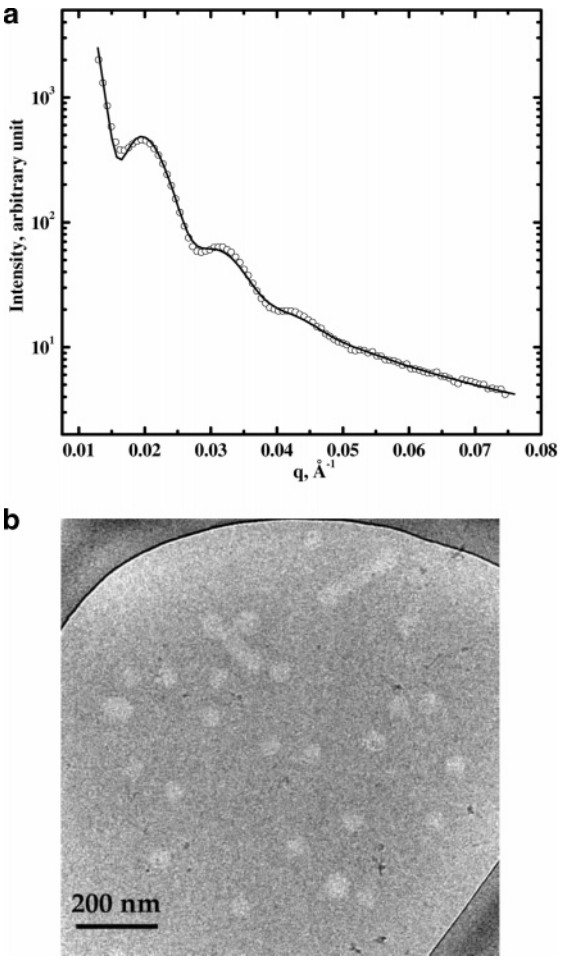

Figure 4. (a) SAXS data showing the form factor of spheres for SI(13-71) in DBP/DEP[3:1] $\phi = 0.01$ (circle) and the fits (solid line). (b) A cryo-TEM image from the corresponding solution.

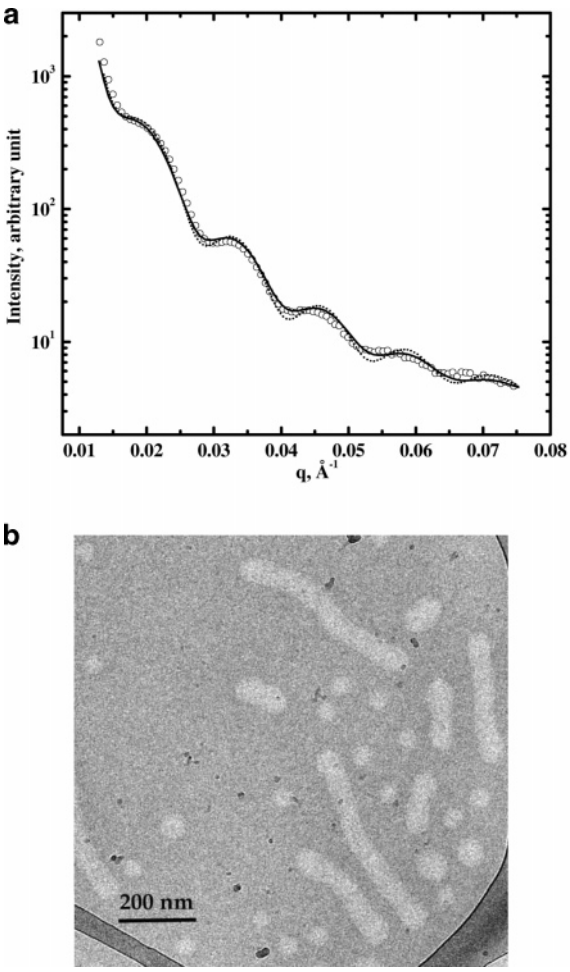

Figure 5. (a) SAXS data showing the form factor of cylinders for SI(13-71) in DBP/DEP[1:1] $\phi = 0.01$ (circle) and the fits (solid and dotted lines). The solid and dotted lines represent the fits with a Gaussian and an exponential distribution, respectively. (b) A cryo-TEM image from the corresponding solution.

data were not converted to an absolute scale. The fit gave $R_c = 29$ nm, $R_g = 3.5$ nm, and $\sigma_R = 4.0$ nm. Note that the core dimension from the characteristic equation for the form factor minima is essentially identical ($R_c = 28$ nm), reflecting the dominance of the core contribution. The cryo-TEM images also show relatively monodisperse spheres (Figure 4b); the average radius of these spheres was in excellent agreement with the core dimension from the fit result.

The solution in DBP/DEP[1:1] was compared with the form factor of cylinders (Figure 5a). As the cryo-TEM images (Figure 5b) revealed relatively short cylinders ($L \leq 500$ nm), the model could not be simplified to the long cylinder case.[39] The polydispersity of the cylinder length, L, with either a Gaussian or an "exponential" distribution was considered. Both fits found the core radius of cylinder R_c to be 25 nm, again in excellent agreement with the estimates from the form factor minima ($R_c = 25$ nm) and the cryo-TEM images.Values of $R_g \approx 3.5$ nm and $d \approx 1$, the same values as for spheres, were assumed for the corona chains, as the fit is insensitive to these parameters. A slightly better fit was obtained with a Gaussian distribution of L (solid line). Also, the fit with the Gaussian distribution gave an average L of 250 nm and a length distribution width σ_L of 180 nm, while a shorter average length (~150 nm) was predicted with the "exponential" distribution. This is probably because of the asymmetry of the latter.

Another aspect to consider in the cylinder fit is the relevant q range. The cylinder form factor is best revealed by the Guinier regime and by the region of q^{-1} power-law dependence, in which L and σ_L can be better determined. For cylinders with $L = 250$ nm and $R_c = 25$ nm, these regimes will lie in the range $q < 0.003$ Å^{-1} and 0.003 Å$^{-1} < q < 0.013$ Å^{-1}, respectively. We do not have access to such q ranges, and hence the determination of L and σ_L is rather indirect, as they were obtained from the smearing of the minima in the form factor and perhaps a few points at the lowest q.

Vesicles have been the subject of numerous studies in lipid systems, due in part to their potential use in biotechnology.[40] Properties of vesicles, such as overall size, size distribution, and layer thickness, have been characterized by SAXS or SANS.[40−47] Vesicles have been modeled as hollow spheres with

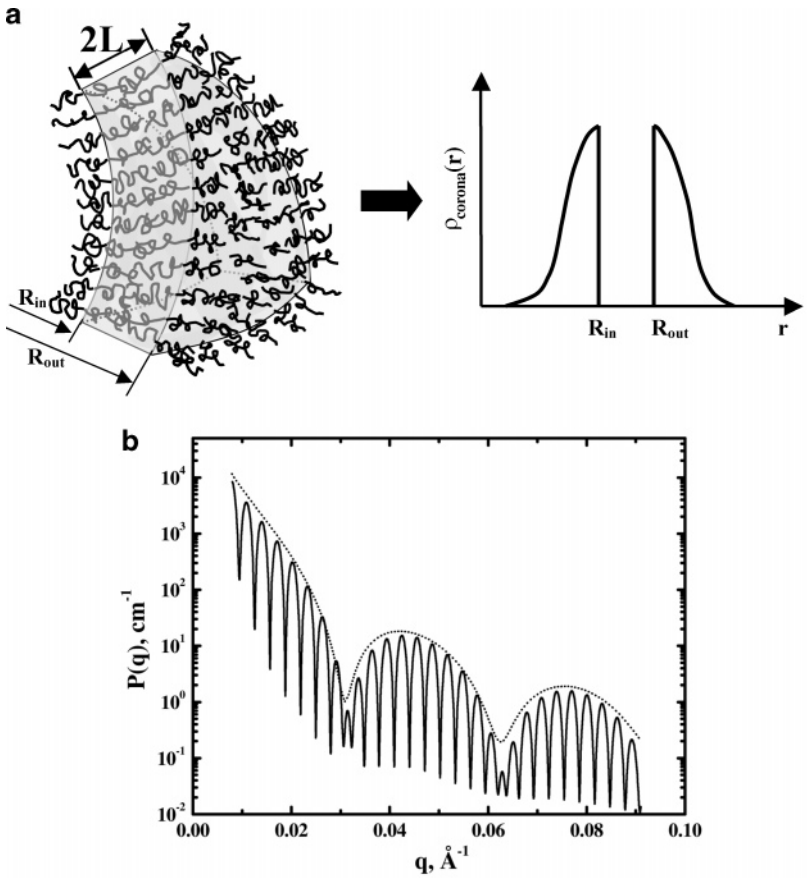

Figure 6. (a) Schematic illustration of the core dimension of a vesicle and density profile of the corona chains across the bilayer. (b) Calculated form factor for a vesicle with $R_c = 100$ nm and $L_c = 10$ nm. The solid and dotted line correspond to monodisperse and polydisperse vesicle sizes, respectively.

a uniform layer thickness. The hollow sphere formula is equivalent to eq 10 without the exponential term. To fit the experimental data, it was found to be necessary to include the polydispersity of the vesicle size in the formula.[42,44] Several approximations to the vesicle form factor have been proposed. For example, Gaussian or Schulz distribution functions were convoluted with the form factor expression.[42,44] In lipid bilayer vesicles, it is also common that the vesicle diameter is much larger than the layer thickness,[43,48] and the form factor expression can be approximated by the form factor for randomly oriented thin sheets, referred to as the Kratky−Porod approximation.[49]

In the case of the vesicle form factor in block copolymers, there are two additional issues to be considered. The first is the relatively thick layers. In lipid vesicles, the layer thickness is typically less than 4 nm. Then, the first minimum in the form factor due to the layer will appear at high q, and, in most cases it was poorly resolved presumably due to the interference from the incoherent background, instrumental smearing, and membrane fluctuations. It is, in fact, also due to a finite width of the interfaces, as it is described with the exponential term. For short surfactant and lipid molecules, the smearing of the interface is significant, and this suppresses the amplitude of the maximum and minimum in the form factor. In contrast, the layer thickness in block copolymer vesicles can be readily adjusted by the molecular weight, and it varies from at least 8 to 40 nm.[50,51] The q range desired for this length scale is approximately between 0.01 and 0.1 $Å^{-1}$, which is easily accessible with small-angle scattering, and the minima from the layer thickness can be depicted. However, in most studies, the block copolymer vesicles have been characterized by TEM,[2,51] as it provides direct information from the images and is a well-established technique in aqueous systems. Another difference arises from the corona chains attached on both sides of the vesicle bilayers. The form factor for the lipid vesicles can be assumed as simple hollow spheres with uniform shell, as the layers usually consist of short hydrophilic headgroups and hydrophobic alkyl chains between headgroups. However, the scattering from the corona chains should also be included in the form factor for the block copolymer vesicles.

In this paper, we modified the hollow sphere model by considering the corona chains. The model was simplified by assuming that the radial profiles of the corona chains on both sides of the layer are symmetric, as illustrated in Figure 6a. We believe this assumption is reasonable because the PS chains in the corona are short compared to the PI core blocks. Also, the SAXS pattern is mainly due to the core scattering, and hence the fit is relatively insensitive to the corona parameters. Figure 6b shows an example of the vesicle form factor with an overall vesicle size $R_c = 100$ nm and a half-layer thickness $L_c = 10$ nm. The same contrast factors as for SI(13-71) in DEP/DMP-[1:1] were used, and the plotted curve reflects the characteristics of the hollow sphere form factor. For monodisperse vesicles (solid line), the form factor features two q-dependent oscillations: a high-frequency oscillation, depending on the vesicle size, and a low-frequency oscillation, corresponding to the layer thickness. The experimental data do not show the rapid oscillations predicted by the form factor because they are smeared out by the polydispersity in vesicle size. With a size distribution width σ_R of 30 nm, the rapid oscillations were completely smeared out, but the slower oscillations were essentially unaffected (dotted line).

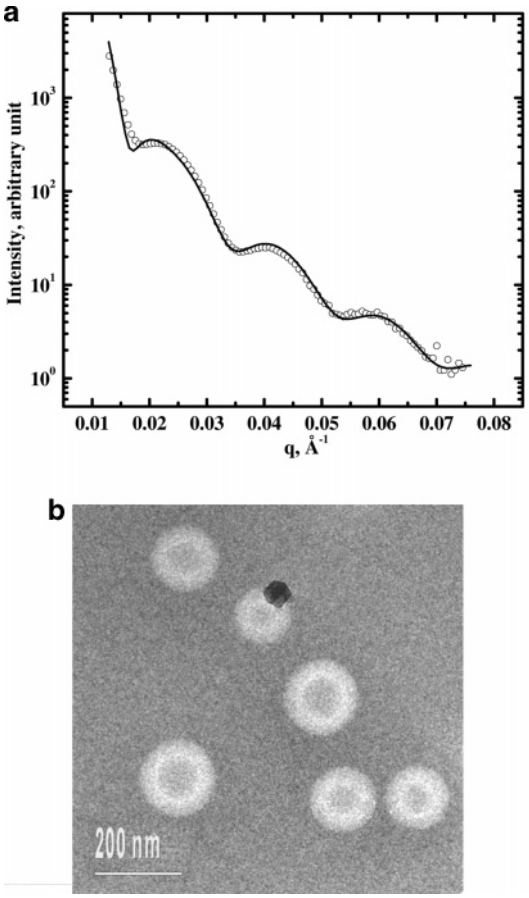

Figure 7. (a) SAXS data showing the form factor of vesicles for SI(13-71) in DEP/DMP[1:1] $\phi = 0.01$ (circle) and the fit (solid line). (b) A cryo-TEM image from the corresponding solution.

The fit result for the DEP/DMP[1:1] solution is shown in Figure 7a. The model gave an excellent fit in that the smearing of the minima was nicely described without considering the polydispersity of the thickness. The best fit was obtained when $R = 46$ nm, $L_c = 18$ nm, and $\sigma_R = 28$ nm. The estimation of L_c from the characteristic equation for the form factor minima was 17 nm, consistent with the fit result. The layer thickness can also be measured from the cryo-TEM images (Figure 7b) by tracing the density profiles across the vesicles. Assuming that the lighter area in the images reflects the layers consisting of the PI blocks, we could also estimate a fairly uniform thickness of 40 nm ($L_c = 20$ nm), showing good agreement with the SAXS data. The cryo-TEM images also revealed the polydisperse distribution in vesicle size, ranging from 30 to 200 nm. It should be pointed out that, as of today, the accurate and simultaneous determination of the vesicle size and the polydispersity is problematic. The most reliable method is probably to incorporate the hard-sphere structure factor.[42] In this case, the peak from the structure factor will appear near $q \approx 10^{-3}$ Å^{-1} for $R_c \approx 100$ nm, which necessitates the use of ultrasmall-angle scattering.

In summary, both cryo-TEM and SAXS were used to determine the aggregate morphologies and provided very consistent results. For SAXS, the detailed micellar structures could be characterized by the relative spacing of the minima in the form factor as well as the model fit. However, we acknowledge that lower q data are required to obtain more reliable information on the overall size and distribution (L and σ_L for cylinders and R and σ_R for vesicles), as discussed above.

Discussion

From the SAXS fit (Figure 5a) and the cryo-TEM images (Figures 1 and 5b), it is apparent that the cylinders are relatively short, compared to the analogous morphologies in aqueous systems. For example, the length of cylinders reported in PB−PEO diblock copolymers in water often exceeds several microns, apparently regardless of molecular weight.[2,21,52] The interaction parameters in this system are estimated to be $\chi_{PB-water} \approx 3.5$ and $\chi_{PB-PEO} \approx 0.4$ (at 25 °C),[2] indicating that the core and corona blocks are strongly segregated and also the core can be assumed as water-free. Under this condition, it is likely that the free energy of an end-cap is high, resulting in a long cylinder. However, the interaction parameter of SI, χ_{PS-PI}, is much lower ($\chi_{PS-PI} \approx 0.09$),[53] and thus the core and corona blocks are less strongly segregated. Also, the interaction parameters between PI and dialkyl phthalates are estimated to be much lower than $\chi_{PB-water}$ and in the range of 0.8−1.8 at 25 °C.[54] For example, the slightly PS selective solvent, DBP, is known to be a Θ solvent for PI in the vicinity of 90 °C,[34,35,55] whereas the Θ temperature of water for PB will be inaccessible. Therefore, it is possible that the core is swollen by the solvent to some extent, as evidenced previously.[12,55] With a less strongly segregated core/corona interface and a swollen core, the free energy difference between an end-cap and the cylinder becomes smaller, and hence the formation of long cylinders is unfavorable.

From the core dimensions (R_c for spheres and cylinders and L_c for vesicles) of each morphology measured from cryo-TEM and SAXS, we can quantify the interfacial area per chain, a_0, and the core chain stretching, s. The values of a_0 and s are summarized in Table 1. Here a_0 was estimated by assuming that there is no solvent in the core, and because some degree of core solvation can be expected, especially in DBP, there will be a tendency to underestimate a_0. A dimensionless parameter, s [$\equiv (R_c \text{ or } L_c)/\langle h \rangle_0$)], can be defined as the ratio of the core dimension, R_c or L_c, to the unperturbed end-to-end distance of the core block, $\langle h \rangle_0$. For the PI block with molecular weight 71 000 g/mol $\langle h \rangle_0 \approx 22$ nm. The core chain stretching, s, decreases from spheres to cylinders to vesicles. From spheres to cylinders to vesicles, both quantities show the expected trend: a_0 decreases from 13, 11, and 8 nm^2/chain, and s also decreases from 1.32, 1.14, and 0.82. Comparing these values with those in aqueous systems, i.e., PB−PEO in water, a_0 is larger and s is smaller.[2] This also reflects the smaller degree of segregation in our system. Also, the molecular weight of the PI core block is at least 10 times larger than that of the PB block reported ($M_{PB} < 5000$ g/mol),[2] which contributes to the significant increase in a_0. One interesting point is that the core chain stretching in the vesicles is less than unity. This could be an indication that the core chains are either partially collapsed or more probably interdigitated across the bilayer, as inferred elsewhere.[40]

A recent paper by Zhulina et al.[56] treats the boundaries between spheres, cylinders, and vesicles in copolymer micelles in detail as a function of the relevant variables. In addition to retaining all three contributions to the free energy (interfacial tension, corona crowding, and core stretching), numerical coefficients are evaluated. Of particular relevance to the work here is the finding that the free energies of the three shapes are very close in the regime of crew-cut micelles, which rationalizes the prevalence of coexisting spheres and cylinders and cylinders and vesicles. Furthermore, the values of the degrees of polymerization of the two blocks in SI(13-71) place this sample exactly in the region where the theory anticipates

the boundaries among the various structures to lie (see Figure 8a of ref 56).

Summary

We have examined the aggregation behavior of a highly asymmetric SI diblock copolymer, SI(13-71), in various dialkyl phthalates with $\phi = 0.01$. The solvent selectivity was tuned by mixing two solvents with various ratios. An increase in the solvent selectivity minimizes the contact between the solvent and the core block and increases the interfacial tension, finally resulting in the aggregate shape changes, from spheres to cylinders to vesicles. The results are analogous to the work of the Eisenberg group, where the solvent selectivity was adjusted by the water content in a mixture of water/DMF or water/dioxane.[6−10] In this context, it can be concluded that the solvent selectivity plays an important role in controlling the micellar morphologies regardless of chemical nature of systems (organic or aqueous).

The aggregate shapes were determined by cryo-TEM and SAXS; both techniques provided equivalent results for the micellar core dimensions. Although cryo-TEM has been established in investigating aqueous solutions, only a few cases have been reported in organic solvents. In this work, we successfully investigated the micellar solutions of dialkyl phthalates. Interestingly, the images consistently exhibit "reverse" contrast, i.e., a lighter core against a darker solvent background. The SAXS data were fitted quantitatively with the corresponding form factors. For spheres and cylinders, the noninteracting Gaussian model was used to describe the corona chains, as the corona contribution is small. The vesicle form factor for the block copolymer was modified from the hollow sphere model by considering the corona chains attached to inside/outside bilayers. These three models described the scattering patterns very well, and the results showed a good agreement with cryo-TEM images. The packing properties a_0 and s were extracted from the core dimensions measured for each micellar morphology. As the aggregate shape changed from spheres to cylinders to vesicles, both a_0 and s decrease. Overall the results are in good agreement with recent theory.

Acknowledgment. This work was supported primarily by the National Science Foundation, through the University of Minnesota MRSEC (DMR-0212302). Portions of this work were performed at the DuPont-Northwestern-Dow Collaborative Access Team (DND-CAT) Synchrotron Research Center located at Sector 5 of the Advanced Photon Source. DND-CAT is supported by the E.I. DuPont de Nemours & Co., The Dow Chemical Company, the U.S. National Science Foundation through Grant DMR-9304725, and the State of Illinois through the Department of Commerce and the Board of Higher Education Grant IBHE HECA NWU 96. Use of the Advanced Photon Source was supported by the U.S. Department of Energy, Basic Energy Sciences, Office of Energy Research, under Contract W-31-102-Eng-38. Some of the cryo-TEM work was performed at the "Hannah and George Krumholz Laboratory for Advanced Microscopy" of the Technion, part of the "Technion Project on Complex Fluids, Microstructure and Macromolecules".

Appendix

The radial profiles of the corona chains inside and outside the bilayers were modeled using a sum of two cubic *b* spline functions. For the sake of simplicity, the profiles inside and outside are assumed to be symmetric (Figure 6a). The profiles can be expressed as

$$\rho_{\text{corona}}(r) = \frac{[\rho_1^{\text{out}}(r) + \rho_1^{\text{in}}(r)] + a_1[\rho_2^{\text{out}}(r) + \rho_2^{\text{in}}(r)]}{1 + a_1} \quad (18)$$

where a_1 is a fitting parameter. $\rho_x^{\text{out}}(r)$ and $\rho_x^{\text{in}}(r)$ represent the cubic *b* splines outside and inside layer, respectively. Then $\rho_1^{\text{out}}(r)$ and $\rho_1^{\text{in}}(r)$ are

$$\rho_1^{\text{out}}(r) = \frac{4(r - R_{\text{out}} - s)^3 - (r - R_{\text{out}} - 2s)^3}{4s^3} \quad \text{for } R_{\text{out}} \le r < R_{\text{out}} + s$$

$$\rho_1^{\text{out}}(r) = \frac{-(r - R_{\text{out}} - 2s)^3}{4s^3} \quad \text{for } R_{\text{out}} + s \le r < R_{\text{out}} + 2s$$

$$\rho_1^{\text{out}}(r) = 0 \quad \text{elsewhere} \quad (19)$$

and

$$\rho_1^{\text{in}}(r) = \frac{-4(r - R_{\text{in}} + s)^3 + (r - R_{\text{in}} + 2s)^3}{4s^3} \quad \text{for } R_{\text{in}} - s \le r < R_{\text{in}}$$

$$\rho_1^{\text{in}}(r) = \frac{(r - R_{\text{in}} + 2s)^3}{4s^3} \quad \text{for } R_{\text{in}} - 2s \le r < R_{\text{in}} - s$$

$$\rho_1^{\text{in}}(r) = 0 \quad \text{elsewhere} \quad (20)$$

For $\rho_2^{\text{out}}(r)$ and $\rho_2^{\text{in}}(r)$,

$$\rho_2^{\text{out}}(r) = \frac{-(r - R_{\text{out}} - s)^3}{s^3} \quad \text{for } R_{\text{out}} \le r < R_{\text{out}} + s$$

$$\rho_2^{\text{out}}(r) = 0 \quad \text{elsewhere} \quad (21)$$

and

$$\rho_2^{\text{in}}(r) = \frac{(r - R_{\text{in}} + s)^3}{s^3} \quad \text{for } R_{\text{in}} - s \le r < R_{\text{in}}$$

$$\rho_2^{\text{in}}(r) = 0 \quad \text{elsewhere} \quad (22)$$

The Fourier transform of the chain profiles above can be calculated to give the scattering amplitude, $A_{\text{corona}}(q)$. They are

$$S_1^{\text{tot}}(q) = C_{\text{norm},1}[S_1^{\text{out}}(q) + S_1^{\text{in}}(q)] \quad (23)$$

where

$$C_{\text{norm},1}^{-1} = \left[\left(\frac{3R_{\text{out}}^2 s}{4} + \frac{7R_{\text{out}}s^2}{10} + \frac{s^3}{4}\right) + \left(\frac{3R_{\text{in}}^2 s}{4} - \frac{7R_{\text{in}}s^2}{10} + \frac{s^3}{4}\right)\right] \quad (24)$$

$$S_1^{\text{out}}(q) = \frac{6\cos[q(R_{\text{out}} + 2s)]}{q^6 s^3} + \left(\frac{3R_{\text{out}}}{2s^3} + \frac{3}{s^2}\right)\frac{\sin[q(R_{\text{out}} + 2s)]}{q^5} - \frac{24\cos[q(R_{\text{out}} + s)]}{q^6 s^3} + \left(\frac{-6R_{\text{out}}}{s^3} - \frac{6}{s^2}\right)\frac{\sin[q(R_{\text{out}} + s)]}{q^5} + \left(\frac{R_{\text{out}}}{q^2} + \frac{3R_{\text{out}}}{q^4 s^2} + \frac{18}{q^6 s^3}\right) \times \cos[qR_{\text{out}}] + \left(\left(\frac{9R_{\text{out}}}{2s^3} - \frac{9}{s^2}\right)\frac{1}{q^5} - \frac{1}{q^3}\right)\sin[qR_{\text{out}}] \quad (25)$$

$$S_1^{\text{in}}(q) = \frac{-24\cos[q(R_{\text{in}}-s)]}{q^6 s^3} + \left(\frac{6}{s^2} - \frac{6R_{\text{in}}}{s^3}\right)\frac{\sin[q(R_{\text{in}}-s)]}{q^5} + \frac{6\cos[q(R_{\text{in}}-2s)]}{q^6 s^3} + \left(\frac{3R_{\text{in}}}{2s^3} - \frac{3}{s^2}\right)\frac{\sin[q(R_{\text{in}}-2s)]}{q^5} + \left(\frac{-R_{\text{in}}}{q^2} - \frac{3R_{\text{in}}}{q^4 s^2} + \frac{18}{q^6 s^3}\right)\times \cos[qR_{\text{in}}] + \left(\frac{1}{q^3} + \left(\frac{9R_{\text{in}}}{2s^3} + \frac{9}{s^2}\right)\frac{1}{q^5}\right)\sin[qR_{\text{in}}] \quad (26)$$

and

$$S_2^{\text{tot}}(q) = C_{\text{norm},2}[S_2^{\text{out}}(q) + S_2^{\text{in}}(q)] \quad (27)$$

where

$$C_{\text{norm},2}^{-1} = \left[\left(\frac{{R_{\text{out}}}^2 s}{4} + \frac{R_{\text{out}} s^2}{10} + \frac{s^3}{60}\right) + \left(\frac{-{R_{\text{in}}}^2 s}{4} + \frac{R_{\text{in}} s^2}{10} - \frac{s^3}{60}\right)\right] \quad (28)$$

$$S_2^{\text{out}}(q) = \frac{24\cos[q(R_{\text{out}}+s)]}{q^6 s^3} + \left(\frac{6R_{\text{out}}}{s^3} + \frac{6}{s^2}\right)\frac{\sin[q(R_{\text{out}}+s)]}{q^5} + \left(\frac{R_{\text{out}}}{q^2} + \left(\frac{6}{s} - \frac{6R_{\text{out}}}{s^2}\right)\frac{1}{q^4} - \frac{24}{q^6 s^3}\right)\cos[qR_{\text{out}}] + \left(\left(\frac{3R_{\text{out}}}{s} - 1\right)\frac{1}{q^3} + \left(\frac{18}{s^2} - \frac{6R_{\text{out}}}{s^3}\right)\frac{1}{q^5}\right)\times \sin[qR_{\text{out}}] \quad (29)$$

$$S_2^{\text{in}}(q) = \frac{24\cos[q(R_{\text{in}}-s)]}{q^6 s^3} - \left(\frac{6}{s^2} - \frac{6R_{\text{in}}}{s^3}\right)\frac{\sin[q(R_{\text{in}}-s)]}{q^5} - \left(\frac{-R_{\text{in}}}{q^2} + \left(-\frac{6R_{\text{in}}}{s^2} - \frac{6}{s}\right)\frac{1}{q^4} + \frac{24}{q^6 s^3}\right)\cos[qR_{\text{in}}] - \left(\left(-\frac{3R_{\text{in}}}{s} - 1\right)\frac{1}{q^3} + \left(\frac{6R_{\text{in}}}{s^3} + \frac{18}{s^2}\right)\frac{1}{q^5}\right)\sin[qR_{\text{in}}] \quad (30)$$

The scattering amplitude can be written as

$$A_{\text{corona}}(q) = \frac{S_1^{\text{tot}}(q) + a_1 S_2^{\text{tot}}(q)}{1 + a_1} \quad (31)$$

References and Notes

(1) Alexandridis, P.; Lindman, B. *Amphiphilic Block Copolymers: Self-Assembly and Applications*; Elsevier Science B.V.: Amsterdam, 2000.
(2) Won, Y.-Y.; Brannan, A. K.; Davis, H. T.; Bates, F. S. *J. Phys. Chem. B* **2002**, *106*, 3354.
(3) Zhang, L.; Eisenberg, A. *Science* **1995**, *268*, 1728.
(4) Halperin, A.; Tirrell, M.; Lodge, T. P. *Adv. Polym. Sci.* **1992**, *100*, 33.
(5) Israelachvili, J. N. *Intermolecular and Surface Forces*; Academic Press: London, 1991.
(6) Shen, H.; Eisenberg, A. *J. Phys. Chem. B* **1999**, *103*, 9473.
(7) Chen, L.; Shen, H.; Eisenberg, A. *J. Phys. Chem. B* **1999**, *103*, 9488.
(8) Zhang, L.; Eisenberg, A. *Macromolecules* **1999**, *32*, 2239.
(9) Shen, H.; Eisenberg, A. *Macromolecules* **2000**, *33*, 2561.
(10) Choucair, A.; Eisenberg, A. *Eur. Phys. J. E* **2003**, *10*, 37.
(11) Canham, P. A.; Lally, T. P.; Price, C.; Stubbersfield, R. B. *J. Chem. Soc., Faraday Trans. 1* **1980**, *76*, 1857.
(12) Pedersen, J. S.; Hamley, I. W.; Ryu, C. Y.; Lodge, T. P. *Macromolecules* **2000**, *33*, 542.
(13) LaRue, I.; Adam, M.; Sheiko, S. S.; Rubinstein, M. *Polym. Mater. Sci. Eng.* **2003**, *88*, 236.
(14) LaRue, I.; Adam, M.; da Silva, M.; Sheiko, S. S.; Rubinstein, M. *Macromolecules* **2004**, *37*, 5002.
(15) LaRue, I.; Adam, M.; Pitsikalis, M.; Hadjichristidis, N.; Rubinstein, M.; Sheiko, S. S. *Macromolecules* **2005**, http://dx.doi.org/10.1021/ma051548z.
(16) Putaux, J.-L.; Minatti, E.; Lefebvre, C.; Borsali, R.; Schappacher, M.; Deffieux, A. *Faraday Discuss.* **2004**, *128*, 163.
(17) Lodge, T. P.; Bang, J.; Li, Z.; Hillmyer, M. A.; Talmon, Y. *Faraday Discuss.* **2004**, *128*, 1.
(18) Kesselman, E.; Talmon, Y.; Bang, J.; Abbas, S.; Li, Z.; Lodge, T. P. *Macromolecules* **2005**, *38*, 6779.
(19) Talmon, Y. *Ber. Bunsen-Ges.* **1996**, *100*, 364.
(20) Pedersen, J. S.; Svaneborg, C. *Curr. Opin. Colloid Interface Sci.* **2002**, *7*, 158.
(21) Won, Y.-Y.; Davis, H. T.; Bates, F. S. *Science* **1999**, *283*, 960.
(22) Jain, S.; Bates, F. S. *Science* **2003**, *300*, 460.
(23) Oostergetel, G. T.; Esselink, F. J.; Hadziioannou, G. *Langmuir* **1995**, *11*, 3721.
(24) Danino, D.; Gupta, R.; Satyavolu, J.; Talmon, Y. *J. Colloid Interface Sci.* **2002**, *249*, 180.
(25) Borsali, R.; Minatti, E.; Putaux, J.-L.; Schappacher, M.; Deffieux, A.; Viville, P.; Lazzaroni, R.; Narayanan, T. *Langmuir* **2003**, *19*, 6.
(26) Lodge, T. P.; Pudil, B.; Hanley, K. J. *Macromolecules* **2002**, *33*, 5918.
(27) Pedersen, J. S.; Gerstenberg, M. C. *Macromolecules* **1996**, *29*, 1363.
(28) Pedersen, J. S. *J. Appl. Crystallogr.* **2000**, *33*, 637.
(29) Pedersen, J. S.; Svaneborg, C.; Almdal, K.; Hamley, I. W.; Young, R. N. *Macromolecules* **2003**, *36*, 416.
(30) Pedersen, J. S.; Gerstenberg, M. C. *Colloids Surf., A* **2003**, *213*, 175.
(31) Bang, J.; Viswanathan, K.; Lodge, T. P.; Park, M. J.; Char, K. *J. Chem. Phys.* **2004**, *121*, 11489.
(32) Castelletto, V.; Hamley, I. W.; Pedersen, J. S. *J. Chem. Phys.* **2002**, *117*, 8124.
(33) Cates, M. E.; Candau, S. J. *J. Phys.: Condens. Matter* **1990**, *2*, 6869.
(34) Hanley, K. J.; Lodge, T. P. *J. Polym. Sci., Polym. Phys. Ed.* **1998**, *36*, 3101.
(35) Hamley, I. W.; Fairclough, J. P. A.; Ryan, A. J.; Ryu, C. Y.; Lodge, T. P.; Gleeson, A. J.; Pedersen, J. S. *Macromolecules* **1998**, *31*, 1188.
(36) Hanley, K. J.; Lodge, T. P.; Huang, C.-I. *Macromolecules* **2000**, *33*, 5918.
(37) Bang, J.; Lodge, T. P. *J. Phys. Chem. B* **2003**, *107*, 12071.
(38) Jain, S.; Bates, F. S. *Macromolecules* **2004**, *37*, 1511.
(39) Won, Y.-Y.; Davis, H. T.; Bates, F. S.; Agamalian, M.; Wignall, G. D. *J. Phys. Chem. B* **2000**, *104*, 7134.
(40) Foerster, S. *Polymer Vesicles: Encyclopedia of Polymer Science and Technology*; John Wiley & Sons: New York, 2005.
(41) Mason, P. C.; Gaulin, B. D.; Epand, R. M.; Wignall, G. D.; Lin, J. S. *Phys. Rev. E* **1999**, *59*, 3361.
(42) Bergstroem, M.; Pedersen, J. S.; Schurtenberger, P.; Egelhaaf, S. U. *J. Phys. Chem. B* **1999**, *103*, 9888.
(43) Lesieur, P.; Kiselev, M. A.; Barsukov, L. I.; Lombardo, D. *J. Appl. Crystallogr.* **2000**, *33*, 623.
(44) Balgavy, P.; Dubnickova, M.; Kucerka, N.; Kiselev, M. A.; Yaradaikin, S. P.; Uhrikova, D. *Biochim. Biophys. Acta* **2001**, *1512*, 40.
(45) Bermudez, H.; Hammer, D. A.; Discher, D. E. *Langmuir* **2004**, *20*, 540.
(46) Pencer, J.; Hallett, F. R. *Phys. Rev. E* **2000**, *61*, 3003.
(47) Battaglia, G.; Ryan, A. J. *J. Am. Chem. Soc.* **2005**, *127*, 8757.
(48) Kiselev, M. A.; Lesieur, P.; Kisselev, A. M.; Lombardo, D.; Aksenov, V. L. *Appl. Phys. A* **2002**, *74*, S1654.
(49) Sadler, D. M.; Worcester, D. L. *J. Mol. Biol.* **1982**, *159*, 485.
(50) Bermudez, H.; Brannan, A. K.; Hammer, D. A.; Bates, F. S.; Discher, D. E. *Macromolecules* **2002**, *35*, 8203.
(51) Soo, P. L.; Eisenberg, A. *J. Polym. Sci., Polym. Phys. Ed.* **2004**, *42*, 923.
(52) Kaya, H.; Willner, L.; Allgaier, J.; Stellbrink, J.; Richter, D. *Appl. Phys. A* **2002**, *74*, S499.
(53) Lodge, T. P.; Pan, C.; Jin, X.; Liu, Z.; Zhao, J.; Maurer, W. W.; Bates, F. S. *J. Polym. Sci., Polym. Phys. Ed.* **1995**, *33*, 2289.
(54) Hanley, K. J. Ph.D. Thesis, University of Minnesota, 2001.
(55) Lodge, T. P.; Xu, X.; Ryu, C. Y.; Hamley, I. W.; Fairclough, J. P. A.; Ryan, A. J.; Pedersen, J. S. *Macromolecules* **1996**, *29*, 5955.
(56) Zhulina, E. B.; Adam, M.; LaRue, I.; Sheiko, S. S.; Rubinstein, M. *Macromolecules* **2005**, *38*, 5330.

MA052023+